EFDA–JET–PR(13)26

C.F. Maggi, E. Delabie, T.M. Biewer, M. Groth, N.C. Hawkes, M. Lehnen,
E. de la Luna, K. McCormick, C. Reux, F. Rimini, E.R. Solano, Y. Andrew,
C. Bourdelle, V. Bobkov, M. Brix, G. Calabro, A. Czarnecka, J. Flanagan,
E. Lerche, S. Marsen, I. Nunes, D. Van Eester, M.F. Stamp
and JET EFDA contributors

L-H Power Threshold Studies in JET with Be/W and C Wall

L-H Power Threshold Studies in JET with Be/W and C Wall

C.F. Maggi[1], E. Delabie[2], T.M. Biewer[3], M. Groth[4], N.C. Hawkes[5], M. Lehnen[6], E. de la Luna[7], K. McCormick[1], C. Reux[8], F. Rimini[5], E.R. Solano[7], Y. Andrew[5], C. Bourdelle[8], V. Bobkov[1], M. Brix[5], G. Calabro[9], A. Czarnecka[10], J. Flanagan[5], E. Lerche[11], S. Marsen[12], I. Nunes[13], D. Van Eester[11], M.F. Stamp[5]
and JET EFDA contributors*

JET-EFDA, Culham Science Centre, OX14 3DB, Abingdon, UK

[1]MPI für Plasmaphysik, EURATOM Association, D-85748 Garching, Germany
[2]Association EURATOM-FOM, Nieuwegein, The Netherlands
[3]Oak Ridge National Laboratory, Oak Ridge, Tennessee 37831, USA
[4]Aalto University, Association EURATOM-Tekes, 02015 Espo, Finland
[5]EURATOM-CCFE Fusion Association, Culham Science Centre, OX14 3DB, Abingdon, OXON, UK
[5]Association EURATOM-FZ, Jülich, Germany
[7]Asociacion EURATOM-CIEMAT, Madrid, Spain
[8]Association EURATOM CEA, IRFM, F-13108 Saint-Paul-lez-Durance, France
[9]Associazione EURATOM-ENEA, Frascati, Italy
[10]Association EURATOM-IPPLM, Poland
[11]LPP-ERM/KMS EURATOM Association, Belgium
[12]MPI für Plasmaphysik, EURATOM Association, D-17491 Greifswald, Germany
[13]Associacao EURATOM-IST, Lisboa, Portugal
** See annex of F. Romanelli et al, "Overview of JET Results", (24th IAEA Fusion Energy Conference, San Diego, USA (2012)).*

Preprint of Paper to be submitted for publication in
Nuclear Fusion

ABSTRACT.
A comparison of the L-H power threshold (P_{thr}) in JET with all carbon, JET-C, and beryllium/tungsten wall (the ITER-like choice), JET-ILW, has been carried out in experiments with slow input power ramps and matched plasma shapes, divertor configuration and I_P/B_T pairs. The low density dependence of the L-H power threshold, namely an increase below a minimum density $n_{e,min}$, which was first observed in JET with the MkII-GB divertor and C wall and subsequently not observed with the current MkII-HD geometry, is observed again with JET-ILW. At plasma densities above $n_{e,min}$, P_{thr} is reduced by ~ 30%, and by ~ 40% when the radiation from the bulk plasma is subtracted (P_{sep}), with JET-ILW compared to JET-C. At the L-H transition the electron temperature at the edge, where the pedestal later develops, is also lower with JET-ILW, for a given edge density. With JET-ILW the minimum density is found to increase roughly linearly with magnetic field, $n_{e,min} \sim B_T^{4/5}$, while the power threshold at the minimum density scales as $P_{sep,min} \sim B_T^{5/2}$. The H-mode power threshold in JET-ILW is found to be sensitive both to variations in main plasma shape (P_{sep} decreases with increasing lower triangularity and increases with upper triangularity) and in divertor configuration. When the data are recast in terms of P_{sep} and Z_{eff} or subdivertor neutral pressure a linear correlation is found, pointing to a possible role of Z_{eff} and/or subdivertor neutral pressure in the L-H transition physics. Depending on the chosen divertor configuration, P_{thr} can be up to a factor of two lower than the ITPA scaling law for densities above $n_{e,min}$. A shallow edge radial electric field well is observed at the L-H transition. The edge impurity ion poloidal velocity remains low, close to its L-mode values, ≤5 km/s ±2-3 km/s, at the L-H transition and throughout the H-mode phase, with no measureable increase within the experimental uncertainties. The edge toroidal rotation profile does not contribute to the depth of the negative E_r well and thus may not be correlated with the formation of the edge transport barrier in JET.

1. INTRODUCTION

In preparation for ITER, JET's main plasma facing components, previously of carbon, have been replaced entirely during one shutdown (2010/2011) with a new ITER-like wall (ILW), with mainly beryllium (Be) in the main chamber and tungsten (W) in the divertor [1]. The main results obtained from the first experimental campaign in JET with the ILW (JET-ILW) are reported in [2], [3]. This paper reports on the experiments aimed at studying the influence of the ILW on the H-mode power threshold, P_{thr}, in particular with respect to modifications in the radiated power and impurity composition compared to JET with the C wall (JET-C) [4]. Such studies are of relevance for ITER, where the available auxiliary heating will be limited and whose predicted P_{thr} is extrapolated from scaling laws of the loss power, P_{loss}, with no account for radiation [5].

Over the years, L-H threshold experiments in JET, as well as in other tokamaks, have found a minimum value of plasma density ($\langle n_e \rangle$), $n_{e,min}$, below which the H-mode power threshold increases with decreasing density (COMPASS [6], [7]; Alcator C-Mod [8], [9]; DIII-D [10]; JET[11],[12]; ASDEX Upgrade [13]). On the other hand, the multi-machine H-mode threshold

scaling law, $P_{thr,08}$ [5], on which current extrapolations for ITER are based, is roughly linear with $<n_e>$ and thus only valid for the so-called 'high density branch' of P_{thr} vs density. The physics mechanisms underlying the 'roll-over' of P_{thr} at low $<n_e>$ remain largely unexplained. On the other hand, recent results from ASDEX Upgrade point to the key role played by the edge ion heat flux as explanation for the strong increase in the L-H power threshold at low density in ECRH heated plasmas [14]. In addition, it is of relevance to ITER, where the transition into H-mode is foreseen at high magnetic field B_T (5.4 T) and at low target L-mode densities to enable H-mode access at the given limited, auxiliary heating power, whether $n_{e,min}$ and $P_{thr,min}$ scale with B_T and machine size. The results reported in this paper address these issues, presenting the experimental evidence recently gained in the JET tokamak.

All discharges reported in this study were conducted in deuterium plasmas and were run with lower single null configuration and (favourable) ion ∇B drift towards the X-point. The loss power at the H-mode transition, P_{thr}, is calculated as $P_{thr} = P_{heat} + P_{OH} - dW_{dia}/dt$, with P_{heat} the auxiliary heating power from either neutral beam heating (NBI) or ion cyclotron resonance heating (ICRH), P_{OH} the Ohmic power and dW_{dia}/dt the rate of change of the diamagnetic stored energy. In order to minimize the uncertainty in the measurement of P_{thr}, in the experiment the additional heating power is increased slowly at a rate of ~ 1 MW/s. In the case of NBI heating, the power ramp is achieved by modulating the NB sources. Although P_{thr} is useful for comparison with the L-H threshold scaling law, the net power across the separatrix, $P_{sep} = P_{thr} - P_{rad,bulk}$ (where $P_{rad,bulk}$ is the radiated power from the bulk plasma) is more likely to be the relevant global physics parameter. In particular, both P_{thr} and P_{sep} need to be quantified when assessing the impact of the change of wall composition (C vs Be/W) on the H-mode threshold. In this study $P_{rad,bulk}$ is the total radiated power measured by bolometry, integrated over the plasma volume to the 98% flux surface. In the following, unless otherwise specified, $<n_e>$ refers to the central line averaged density, which in JET is measured along the central chord of the FIR interferometer [15]. In line with earlier JET analyses, all global parameters are averaged over a time interval of 50 ms in the L-mode phase before t_{L-H}, the time of the L-H transition.

The paper is organized as follows: Section 2 summarizes the main results obtained in past L-H threshold experiments in JET-C with different divertor geometries. More recent L-H transition experiments at low density, carried out in 2008/2009 in JET-C with the current MkII-HD geometry, are also reported [16]. Section 3 addresses the findings obtained in 2011/12 with JET-ILW. Section 4 compares the evolution of JET-ILW and JET-C plasmas after the L-H transition. Section 5 studies the edge radial electric field at the L-H transition in relation to variations in the global parameters known to affect P_{sep}, namely $<n_e>$, magnetic field B_T, divertor configuration and plasma wall composition. Summary and conclusions are drawn in Section 6.

2. L-H POWER THRESHOLD IN JET WITH C WALL

2.1. DEPENDENCE OF P_{thr} AND EDGE T_e ON PLASMA DENSITY, MAGNETIC FIELD AND DIVERTOR GEOMETRY

The ITPA scaling law for the H-mode power threshold, $P_{thr,08} \sim \langle n_e \rangle^{0.717}\ B_T^{0.803}\ S^{0.94}$ [5], is recognized as only being valid for medium to high densities, as many tokamak experiments have observed an increase in P_{thr} and edge T_e ($T_{e,edge}$) with decreasing $\langle n_e \rangle$, below a minimum density, $n_{e,min}$ [5]. In JET-C this was first observed with the MarkII Gas Box (MkII-GB) divertor geometry [11], [12] at B_T values of 2.4-2.7 T. Here we define edge T_e and n_e as the values of the electron temperature and density at the radial position where the pedestal top is found in the established H-mode phase. The edge T_e is measured by fast ECE [17] and high resolution Thomson scattering (HRTS) [18], while the edge n_e is measured by the outermost vertical chord of the far infrared interferometer [15] and is directly proportional to the electron density at the top of the pedestal in H-mode. The MkII-GB divertor geometry was a closed geometry with respect to recycling neutrals and was characterized by the presence of a septum, separating the inner and outer divertor legs. The magnetic configurations were typically run with inner and outer strike points on the vertical targets (Fig.1a). Subsequently, a modified version of the MkII-GB geometry was implemented in JET-C, by removing the divertor septum, the so called MkII-GB Septum Replacement geometry, MkII-GB SRP, (Fig.1b). L-H threshold experiments were repeated with this divertor geometry, but in this case no 'roll-over' of P_{thr} and edge T_e at low density were found [12]. Rather, a roughly linear decrease of P_{thr} with decreasing density was observed (Fig.7a in [12]) and it was speculated that removal of the divertor septum may have lowered the density turning point of P_{thr}. The edge electron temperature at the L-H transition was found to vary weakly with edge electron density (Fig.7b in [12]), in contrast to the strong increase of edge T_e at low $\langle n_e \rangle$ observed with the MkII-GB divertor [11], [12].

More recently, in 2008/2009, L-H transition experiments were carried out in JET-C with the currently installed MkII-HD divertor geometry (Fig. 1c) at two values of magnetic field, 1.8T/1.7MA and 3.0T/2.75MA, at constant $q_{95} = 3.4$ [16]. Broad agreement between P_{thr} and $P_{thr,08}$ was observed both at low and high magnetic field, as illustrated in Figures 2a and b, although the measured P_{thr} is systematically higher than the scaling law prediction at $B_T = 3.0$T. The dataset at $B_T = 1.8$ T includes discharges with low and high triangularity shape, $\delta = 0.24$ and $\delta = 0.36$ respectively, whereas the dataset at $B_T = 3.0$T was run with high δ shape only ($\delta = 0.36$). The variation in triangularity introduces only a small variation in P_{thr} at low field, which is not further investigated here. At both fields the discharges were heated with a combination of NBI and ICRH heating and with ICRH only at the lowest densities. Although P_{thr} is similar in plasmas with NBI or ICRH heating, small (10-20%) but systematic variations in P_{thr} are observed as a result of changes in the additional momentum input (by means of modifications of the NBI/ICRH ratio), accounting for some of the scatter in the data of Figs. 2a and 2b. We note that in DIII-D P_{thr} is found to increase with injected torque and edge toroidal rotation in experiments that vary input power and torque independently by means of co- and counter- NBI [19].

In any case, P_{thr} monotonically decreases with decreasing $<n_e>$ and does not 'roll-over' at low density with the MkII-HD geometry in JET-C. In addition, the edge T_e at the L-H transition remains roughly constant - apart from an increase at the lowest density in the 1.7MA/1.8T dataset - as the edge line averaged density is varied across a range of values similar to those of the experiments with the MkII-GB divertor geometry (see Fig. 7b in [12]), as shown in Figure 3. Thus it is possible that changes in the JET divertor geometry have led to a shift of $n_{e,min}$ towards lower densities, which are not accessible experimentally due to the onset of locked modes in the discharge.

In summary, in JET-C the L-H threshold dataset at low density covers a variation in magnetic field values of roughly a factor of two, essentially the JET working B_T range, and spans different divertor geometries. The occurrence of a minimum in P_{thr} with density is not a universal feature in JET-C, but is observed to be sensitive to changes in the divertor geometry, pointing to a strong role of the edge and divertor physics in the L-H transition. This observation is of great significance in view of extrapolation of results from present day tokamaks to ITER. In particular, we note that the JET MkII-HD geometry and the ITER divertor geometry are quite different.

2.2. DEPENDENCE OF P_{thr} AND EDGE T_e ON PLASMA CURRENT OR q_{95}

L-H threshold experiments at low density in JET-C with the MkII-GB divertor had shown the loss power and the edge electron temperature at the H-mode transition to increase weakly with plasma current, I_P, or safety factor q_{95}, for fixed toroidal field [11]. At B_T = 2.4 T and low density, $<n_e>$ = 2.0 x 10^{19} m^{-3}, P_{thr} varied as $P_{thr} \sim I_P^{\alpha}$, with $|\alpha| < 0.2$, when I_P was varied from 2.0 to 3.0 MA in the experiment [11]. This is consistent with the absence of an I_P dependence in the $P_{thr,08}$ scaling law [5] and in the H-mode power threshold data of Alcator C-Mod [9].

More recently, in a plasma current scan carried out in JET-C with the MkII-HD divertor at constant B_T = 3.0 T and $<n_e> \sim 2.0\text{x}10^{19}$ m^{-3}, P_{thr} was found to vary weakly with I_P (or q_{95}), as shown in Figure 4, $P_{thr}/P_{thr,08} \sim I_P^{0.2}$, thus confirming the earlier findings. In these more recent experiments I_P was varied from 1.7 to 2.75 MA, with a corresponding variation in q_{95} from 5.7 to 3.4. In Figure 4 P_{thr} has been normalized to $P_{thr,08}$ to account for the ~ 20% increase in plasma density as the plasma current is raised from low current ($<n_e>$ = 1.6 x 10^{19} m^{-3} at 1.7 and 2.0 MA) to 2.75 MA ($<n_e>$ = 2.1 x10^{19} m^{-3}). The weak dependence of P_{thr} on plasma current or q_{95} appears to be robust against variations in divertor geometry in JET-C.

3. L-H THRESHOLD IN JET WITH BE/W WALL

3.1. DENSITY DEPENDENCE, PLASMA IMPURITY COMPOSITION AND RADIATION

In order to separate the influence of changes in plasma facing components on the L-H power threshold from those related to other parameters known to affect P_{thr}, such as the main plasma shape and/or the divertor geometry, L-H transition experiments have been carried out in JET-ILW with I_P/B_T pairs and plasma shapes matched to those of the L-H discharges in JET-C with the MkII-HD divertor geometry. The plasma density was varied from pulse to pulse, so as to obtain

an overlap in density range with the JET-C dataset. As in the experiments performed with JET-C, slow input power ramps (ICRH or NBI), typically 1 MW/s, were used to measure P_{thr}. In the discharges with ICRH heating at 1.8T, the 2nd harmonic Hydrogen minority heating scheme (f = 32.5 MHz) was used.

At 1.8T/1.7MA and low triangularity (δ = 0.25), both P_{thr} and P_{sep} are found to increase below a minimum density, $n_{e,min} \sim 2.2 \times 10^{19}$ m^{-3}, as shown in Fig. 5, thus recovering the low density dependence first observed in JET-C with the MkII-GB divertor. At plasma densities above $n_{e,min}$, P_{thr} is reduced by ~ 30% and P_{sep} by ~ 40% with Be/W wall compared to JET-C. A similar, strong influence of the change in wall composition on P_{thr} and P_{sep} is also observed for the dataset at 3.0T/2.75MA and high triangularity (δ = 0.35), as shown in Fig. 6. In addition, we observe that $n_{e,min} \sim 3.5 \times 10^{19}$ m^{-3} at 3.0 T, having increased roughly linearly with B_T (at constant q_{95}). This finding will be discussed in more detail in section 3.3.

In JET-ILW, a sharp increase in P_{thr} is found for plasma densities below $n_{e,min}$ in ICRH heated discharges (Fig. 5 a). This is due to the strong increase in $P_{rad,bulk}$ at low density, as shown in Figure 7. On the other hand, after subtraction of the core radiation, similar values of P_{sep} are found in NBI and ICRH heated discharges at a given density (Figure 5 b). Thus, the L-H power threshold is independent of heating method in JET-ILW, but more input power is required in JET-ILW than in JET-C to access the H-mode at low density, due to increased core radiation at very low densities. Similar radiated power fractions are measured at the L-H transition, for a given density, in JET-C and JET-ILW NBI heated discharges, while the JET-ILW ICRH heated discharges differ strongly, both from the NBI heated JET-ILW dataset and from the JET-C dataset, showing a drastic increase in $P_{rad,core}/P_{loss}$ with decreasing density (see [20] for further details on ICRH heating in JET-ILW). This is illustrated in Figure 7 by the radiated power normalized to P_{loss} at the L-H transition for the set of discharges at 1.8T/1.7MA, where we separate core (solid symbols) and divertor + X-point (open symbols) contribution to the total radiated power. W and Ni are the main intrinsic core radiators, as measured by XUV spectroscopy, with W contributing to roughly 80% of $P_{rad,bulk}$. Both W and Ni concentrations increase strongly with decreasing density and in either case higher concentrations are found in ICRH than in NBI heated discharges. The W concentration, measured from the quasi-continuum spectrum at 5 nm [21], increases from ~ 1.0×10^{-5} at $\langle n_e \rangle = 3\times10^{19}$ m^{-3} to ~ 1-2 x 10^{-4} at $\langle n_e \rangle = 1.5 \times 10^{19}$ m^{-3} with ICRH heating and low D_2 fuelling in the dataset.

The line averaged Z_{eff} is strongly reduced from JET-C to JET-ILW due to: i) the strong reduction in C concentration after the transition to full metal wall [22], $c_C \sim$ 0.5-1 % in JET-C to $c_C \sim$ 0.05% in JET-ILW, as measured by edge CXRS at the L-H transition; ii) the reduction in Z of the main intrinsic impurity (Be) and iii) the absence of chemical sputtering for Be. Figure 8 shows a comparison of the line averaged Z_{eff} for the JET-C and JET-ILW L-H data sets of Figures 5 and 6. Statistical error bars are shown (10%), while a systematic error of 20% should be considered when comparing JET-C with JET-ILW datasets. The strongest reduction in Z_{eff} due to the change from JET-C to all metal wall is observed for the plasmas at high triangularity. It is not yet clear if

this reduction in Z_{eff} is linked to the changes in power threshold and edge temperature observed in JET-ILW compared to JET-C at the L-H transition.

Together with a reduction in P_{sep}, we find that at a given edge density the L-H transition occurs at lower edge electron temperature, and thus lower electron pressure, with JET-ILW than with JET-C, as shown in Figure 9 a) and b) for the datasets at 1.8 T and 3.0 T, respectively. In NBI heated discharges, where $T_{i,edge}$ can be measured with edge CXRS, $T_{i,edge}$ and $T_{e,edge}$ are strongly coupled over the explored density range down to the lowest densities, both in JET-C and JET-ILW (see Section 5), as shown in Figure 9 c). The ratio $T_{i,edge}/T_{e,edge}$ is ~ 1 for the entire density scan, hence indicating that also $T_{i,edge}$ varies weakly with edge density. For the JET-C dataset, the edge T_i data are of poorer quality, but a similar trend is observed as in JET-ILW. For the 1.8 T data, we note that the combined effect of lower edge T_e and lower Z_{eff} at the L-H transition in JET-ILW, compared with JET-C, leads to similar values of edge resistivity in the two cases for a given density (where the edge resistivity is $\eta = 2.8 \times 10^{-8}\, Z_{eff}/T_{e,edge}^{3/2}$ Ωm, $T_{e,edge}$ [keV], $\ln\Lambda = 17$ [23]), but to up to a factor of two higher edge collisionality ν_e^* in the JET-ILW dataset. The edge collisionality here is the ion-electron collision frequency normalized to the bounce frequency as in [24] calculated at the radial position corresponding to the pedestal top in the H-mode phase. It can be written as $\nu^* = 0.001\, Z_{eff}\, n_e\, R\, q_{95}/(T_e^2\, \varepsilon^{3/2})$, with T_e [keV], n_e [10^{19} m^{-3}], ε the inverse aspect ratio and R the major radius. For the 3.0 T data similar values of edge resistivity and collisionality are found in JET-C and JET-ILW in the region of overlap in edge plasma density, while the higher density branch of the JET-ILW dataset drives to a 50% increase in edge resisitivity and to a factor of 3 increase in edge collisionality at the highest density point. These observations may be useful in comparisons of the experimental findings with theoretical models of the H-mode barrier formation.

Finally, we note that in ASDEX-Upgrade the full transition to all-W wall has also led to a decrease of the L-H power threshold, normalized to the ITPA scaling [5], $P_{thr}/P_{thr,08}$, of order 25% in the high density branch of P_{thr} [3]. Given that i) the JET and AUG divertor geometries are quite different and ii) the main plasma wall components are also different (Be for JET, W for AUG) there is some degree of confidence in the extrapolation of this result to ITER. It may be that the observed reduction of P_{thr} in the high density branch could be related to the absence/strong reduction of C concentration in the edge plasma (through changes in radiation profile and/or effective mass).

3.2. DEPENDENCE OF L-H POWER THRESHOLD ON DIVERTOR GEOMETRY AND PLASMA SHAPE

Dedicated experiments were also carried out in JET-ILW to study the sensitivity of the L-H power threshold to variations in divertor configuration and main plasma shape, which are known hidden parameters not included in the multi-machine scaling laws for P_{thr}. Five different magnetic configurations were explored at B_T/I_P = 2.4 T/2.0 MA (q_{95} ~3.8), as listed in Table 1, in order to decouple variations in divertor configuration from variations in main plasma shape. The lower (δ_L) and upper (δ_U) triangularity are taken as proxy for the divertor configuration and the main plasma

shape, respectively. Three configurations were investigated with the main plasma shape kept fixed (high upper triangularity, $\delta_U \sim 0.38$) while the divertor configuration was varied by moving the strike points from left to right of the divertor floor (configurations locally known at JET as HT3L, HT3R and HT3, see Figure 10). This change in divertor configuration is obtained by decreasing the lower triangularity δ_L from 0.41 to 0.33. Two companion configurations kept the main plasma shape fixed at low upper triangularity, $\delta_U \sim 0.19$, and varied the lower triangularity δ_L to match the divertor configurations of the HT3L and HT3R shapes (configurations locally known at JET as V5L and V5). As the outer strike point is moved from left to right on the horizontal plate and the inner strike point is moved down along the vertical plate (i.e. with decreasing δ_L), the divertor pumping increases (see Figure 10 d) and the divertor volume becomes less open to recycling neutrals escaping to the main chamber.

In a first set of experiments, run at fixed target density $\langle n_e \rangle = n_{e,min}$, P_{sep} is found to decrease linearly with increasing δ_L at fixed upper triangularity and to increase by ~ 25% as δ_u is raised from ~ 0.19 to ~ 0.38, at fixed divertor configuration, as shown in Figure 11 a. When the data are recast in terms of P_{sep} and Z_{eff}, a linear correlation is found (at constant edge density), as shown in Figure 11 b, pointing to a possible role of Z_{eff} in the L-H transition, as proposed in [25]. P_{sep} is also clearly correlated with the neutral pressure in the subdivertor region (as measured with the recently installed baratron absolute pressure gauge, see [26] and Figure 10 d for the geometrical location of the measurement) as shown in Figure 11 c, indicating that this parameter may also be playing a role in the L-H transition physics.

In a second set of experiments, low density scans were performed in the two low δ shapes (V5 and V5L, as illustrated in Figure 12 b), while keeping the main plasma shape fixed. Depending on the chosen divertor configuration (δ_L), P_{thr} can be up to a factor two lower than the scaling law $P_{thr,08}$ for densities above $n_{e,min}$, as indicated in Figure 12 a. These results are indicative of a possible role of scrape-off-layer physics in the L-H transition, e.g. through changes in recycling and/or scrape-off layer flows.

Finally, we note that, in contrast to the measurements reported here, in earlier JET-C experiments with the MkII-GB SRP geometry as δ_U was raised from 0.23 to 0.34, with δ_L and divertor configuration kept constant, no effect on P_{thr}, nor on edge T_e and T_i at the L-H transition was observed [27]. Thus, it appears that the change in wall composition from JET-C to JET-ILW has resulted in enhanced sensitivity of the H-mode power threshold to variations in main plasma shape.

3.3. DEPENDENCE OF $N_{e,min}$ AND $P_{sep,min}$ ON TOROIDAL MAGNETIC FIELD

It is relevant to ITER whether (and how) the density at which the minimum in P_{thr} occurs, $n_{e,min}$, varies with B_T. Analysis of the data submitted to the international H-mode threshold database suggests the following trend for $n_{e,min}$ [5]: i) $n_{e,min}$ increases with B_T in JET and JT-60U, ii) $n_{e,min}$ is higher in AUG and DIII-D than in JET and JT-60U by about a factor of two, iii) C-Mod, operated

at significantly higher B_T than the other tokamaks, exhibits a very high $n_{e,min}$, which, if confirmed, would imply an unfavourable B_T dependence for ITER.

As described in the previous sections, the L-H experiments with JET-ILW were carried out at 3 different values of B_T, thus providing additional data from JET on the variation of $n_{e,min}$ and $P_{sep,min}$ with B_T. Figure 13 (a) shows that $n_{e,min}$ increases roughly linearly with B_T in JET-ILW: $n_{e,min} \sim B_T^{4/5}$. Figure 13 (b) indicates that $P_{sep,min}$ increases more strongly than linearly with B_T: $P_{sep,min} \sim B_T^{5/2}$. However, as highlighted in Section 3.1, the occurrence of a minimum in P_{thr} with density is not a universal feature in JET: it is observed to be sensitive to changes in the divertor geometry in JET-C and to changes in the wall composition (C vs Be/W) for a given divertor geometry (MkII-HD). These findings make extrapolations to ITER even more challenging until a physics-based model predicting such observations is identified. Finally, a multi-machine comparison should reveal the scaling of $n_{e,min}$ and $P_{sep,min}$ with B_T/R, where R is the plasma major radius. In particular, a combined analysis of the JET and C-Mod data [9] should be sought, as the results from the two machines are well paired and in view of the absence of a B_T dependence of $P_{sep,min}$ in C-Mod at high magnetic field (3.5 to 5.4 T), as reported in [9].

4. PLASMA EVOLUTION AFTER THE L-H TRANSITION WITH C AND BE/W WALL

In JET the L-H transition at low density has never appeared as a clear bifurcation. Rather, as the power is slowly increased, the plasmas evolve smoothly from a state that is clearly L-mode to one which is clearly H-mode, with a gradual increase in the energy and particle confinement. A similar phenomenology has also been observed in JET-ILW. However, in JET-ILW weaker edge transport barriers are formed after the L-H transition, leading to weaker rates of change in stored energy and, typically, to H-modes with poorer confinement factors than in JET-C. This is illustrated in Figure 14, with time traces for two NBI-heated discharges, one in JET-C (red traces) and one in JET-ILW (blue traces), at similar central line averaged densities in the high density branch of the P_{sep}-n_e space of Figure 5. In addition, JET-ILW plasmas heated by ICRH only or by low levels of NBI remain quiescent after the L-H transition, with no ELM activity. In the high density branch of the P_{sep} - $\langle n_e \rangle$ space and with NBI heating, divertor oscillations [28] are observed in the L-mode phase prior to the L-H transition, while ELM activity appears after the L-H transition.

Indeed, analysis of a database of JET-C and JET-ILW fully developed ELMy H-modes shows that the latter are generally characterized by lower pedestal temperatures for similar pedestal densities [29]. Further experiments are planned in upcoming campaigns to try and expand the operating space of JET-ILW and good H-mode confinement on one hand, while modelling activities are ongoing in order to identify the physics mechanism underlying this difference and thus enable extrapolations to ITER. We also note that H-mode pedestal pressures similar to those obtained in JET-C can be restored in the presence of N_2 seeding at high triangularity [30]. Also, the slower ELM dynamics, typical of unseeded JET-ILW H-modes, is modified towards JET-C characteristics when N_2 seeding is applied [29]. Thus it is possible that the strong reduction of intrinsic carbon impurities

in JET-ILW has modified the edge MHD stability of these plasmas, resulting in degraded pedestal pressures. Also planned for the upcoming JET experimental campaigns are L-H transitions in the presence of N_2 seeding, to test if P_{thr} and $T_{e,edge}$ values typical of JET-C plasmas can be recovered when similar Z_{eff} and radiation profiles are re-established in JET-ILW.

5. LOCAL ANALYSIS: EDGE RADIAL ELECTRIC FIELD AT THE L-H TRANSITION

The leading theory for the L-H transition and the formation of the H-mode edge transport barrier is that a critical *ExB* shear is needed to suppress L-mode turbulence and trigger the transition to H-mode. Thus, analysis of the edge ion pressure profiles and flows and their relation to the global measurement, the L-H threshold power, is called for. In this section we examine the edge radial electric field in JET across the L-H transition.

The edge radial electric field, E_r, is calculated from the C^{+6} impurity force balance equation, $E_r = \nabla p_I/(Ze\, n_I) + v_{pol}\, B_{tor} - v_{tor}\, B_{pol}$, where p_I and n_I are the impurity pressure and density, Z the charge state and e the elementary charge, v_{pol} and v_{tor} the poloidal and toroidal velocity, measured by edge CXRS on C^{+6} [31] and B_{pol} and B_{tor} the poloidal and toroidal magnetic field. The JET edge CXRS diagnostic has been refurbished prior to the ILW experimental campaign, leading to profile data with improved time (10 ms) and spatial (~ 1.5 cm) resolution. In addition, the entire optical path of the diagnostic could be absolutely calibrated for the first time by means of in-vessel calibrations, which in JET can only be achieved with remote handling, as described in [32]. This technique has enabled improved accuracy in the edge impurity density measurements compared to the past.

The C^{+6} poloidal velocity is found to be of order 0-5 ± 2-3 km/s at the L-H transition and remains at this low magnitude with no sign of evolution outside the experimental error bars during the H-mode phase of the discharges analysed. The experimental uncertainty in v_{pol} is dominated by poor photon statistics in the near-separatrix region, where the C^{+6} CX signal is very weak. Some improvement on this can be obtained by frame averaging of the CX spectra over a time interval of 100 ms, as in the case of Figure 15, which shows v_{pol} obtained in the steady L-mode phase prior to the L-H transition for a JET-ILW discharge at 3.0T/2.75MA. Given the low values of edge poloidal velocities measured in JET, a further reduction of the experimental uncertainty is necessary in order to enable measurement of the evolution of v_{pol} across the L-H transition and during the H-mode phase. Such low values of v_{pol} are consistent with previous measurements of poloidal velocity from JET [33], [34], but in contrast to observations from other tokamaks, where poloidal velocities of significant magnitudes have been measured in H-mode (see e.g. [35] for recent results on ASDEX Upgrade). Comparison of the JET-ILW v_{pol} measurements with predictions from neoclassical theory is the subject of a future work.

Examples of edge ion density, temperature and toroidal rotation profiles at the L-H transition are shown in panels (a), (b) and (c) of Figure 16 for a JET-ILW discharge at 3.0T/2.75MA (the point at highest density in the dataset of Figure 6), together with *mtanh* fits [36] to the data. For

comparison, panels (d), (e) and (f) illustrate the evolution of the same edge parameters 10 ms after the L-H transition (i.e. for the subsequent edge CXRS data frame). Panels (b) and (e) also show the edge electron temperature profiles from fast ECE. A steepening of the edge gradients, associated with the formation of the edge transport barrier after the L-H transition, is observed in all profiles, but is more pronounced in the density and toroidal rotation profiles. Weak ion and electron temperature pedestals are formed after the L-H transition in JET-ILW, as described in Section 4. The fit to the ion temperature profile in the proximity of the separatrix has been adjusted slightly to follow the electron temperature profile, as derivation of ion temperature data becomes very uncertain in this region due to C^{+6} charge exchange spectra of very weak intensity. Very low values of toroidal rotation are measured in the edge temperature and density gradient region, where the profile has therefore been set to zero by the *mtanh* fit. The ion density profile is instead more accurate, being derived from spectral line intensities rather than their widths. Due to uncertainties in the EFIT equilibrium reconstructions, alignment of the edge profiles with respect to the separatrix position is inaccurate when projected at the torus outer midplane. The relative alignment of the edge profiles with respect to the separatrix position is thus improved by invoking pressure balance along the magnetic field lines. However, after this correction, a residual uncertainty of order 0.5 cm still remains in the separatrix position.

Both in JET-ILW, as shown in Figure 16, and in JET-C the ion and electron temperatures are tightly coupled at the L-H transition throughout the data set, down to the lowest densities. This is unlike the case of the ASDEX Upgrade ECRH heated L-H transitions at low density, where strong decoupling of the ion and electron channels is achieved [37]. We note that at the auxiliary heating powers, heating schemes and edge temperatures involved in the JET L-H experiments, the ion and electron channels are heated in roughly equal proportions, both for the NBI and the ICRH heated discharges. As shown in Figures 3 and 9, the edge temperature varies weakly with edge density at the L-H transition. This is in contrast to the earlier measurements with the MkII-GB divertor in JET-C, where $T_{e,edge}$ at the L-H transition increased strongly with decreasing n_e [11], [12].

Figure 17 shows the edge radial electric field, E_r, calculated from the edge profiles of Figure 16 and assuming $v_{pol} = 0 \pm 2.5$ km/s (solid black line: E_r ($v_{pol} = 0$); dashed black lines: upper and lower bounds of E_r derived from the uncertainty in the v_{pol} measurement). The large error bars in v_{pol}, coupled to its low values, imply a large uncertainty in the $v_{pol}\, B_{tor}$ term of E_r. This prevents the evaluation of the overall depth of the E_r well and of the relative strength of diamagnetic vs poloidal velocity terms in the radial force balance of impurity ions. Despite these limitations, a few observations can be made on the relative dynamics of E_r across the L-H transition - panels (a) and (b) - and in the H-mode phase at the end of the NBI heating ramp - panel (c). At the L-H transition – panel (a) - a shallow E_r well is observed: the weak impurity ion diamagnetic term has a depth of order 2kV/m, while the toroidal rotation term does not appear to contribute to the E_r well, but is the dominant contributor to the E_r shear more radially inwards. Panel (b) shows the evolution of the E_r profile 10 ms after the L-H transition: all gradients have steepened, in particular the ion density

gradient (Figure 16 d), and the E_r well has become deeper, by about a factor of two, compared to the previous time frame. The diamagnetic term of the negative E_r well increases in magnitude in the radial region where the edge density and temperature transport barriers have formed, whereas the increased gradient driven by the toroidal rotation profile is localized radially inwards of the pedestal top. Therefore, the diamagnetic term is likely to be correlated with the formation of the H-mode pedestal at the L-H transition while the $v_{tor} B_{pol}$ term is not likely to be. This hypothesis is consistent with the observation that no significant difference in P_{thr} is found in JET between NBI heated (with additional momentum input) and ICRH heated (no additional momentum input) L-H transitions. Moreover, L-H experiments with significant variations in toroidal field ripple, which in turn induced significant changes in the edge toroidal rotation, had no effect on the L-H power threshold [38]. In other words, the E_r shear driven by the toroidal rotation profile does not appear to be playing a role in setting the edge transport barrier in JET. For comparison, panel (c) shows the E_r profile during the ELMy H-mode phase of the discharge at the end of the input power ramp (P_{in} = 8 MW), where a deeper E_r well is observed.

In summary, our edge profile analysis indicates that only the diamagnetic term $E_{r,dia}$ of the C^{+6} impurity force balance equation shows a sizeable evolution across the L-H transition and into the H-mode phase. Any evolution of v_{pol} across the L-H transition and even into the H-mode phase cannot be measured at present and would require a substantial reduction of the experimental uncertainties. Since edge CXRS data are not available for the entire L-H dataset of this work (and absent for the ICRH only heated discharges), we can extend the analysis of $E_{r,dia}$ to the whole L-H data set using the edge electron kinetic profiles, under the assumption of constant Z_{eff} and $T_i = T_e$ (which is verified experimentally near the pedestal top region). The T_e profiles are obtained from *mtanh* fits to the HRTS and ECE data, while the n_e profiles from *mtanh* fits to the Li-beam [39] and HRTS data for low δ discharges and from *mtanh* fits to the HRTS data only in high δ discharges. For the discharges where both electron and edge CXRS data are available, very similar $E_{r,dia}$ profiles are obtained using the two methods. Throughout the data set we find a very shallow $E_{r,dia}$ at the L-H transition, with a minimum value of order - (1-3) kV/m. No systematic variation of $E_{r,dia}$ is found with edge density, toroidal magnetic field, divertor configuration nor wall composition (JET-C and JET-ILW), except possibly for deeper $E_{r,dia}$ wells at 3T than at 1.8T at low density, which cannot be excluded by the data and would need to be tested further by a larger dataset. Recasting the data in terms of the ExB flow, $v_E = E_{r,dia}/B$, as shown in Figure 18, leads to a fairly constant value across the range of parameters explored, indicating that the ExB flow, rather than the negative E_r, may be the parameter behind the physics of the L-H transition. On the other hand, the global analysis presented in this work shows significant variations in P_{thr} as a function of edge density, toroidal magnetic field, divertor configuration and wall composition. The 'local' and the 'global' observations could be linked under the assumption that a critical negative E_r value or ExB flow must be achieved for the L-H transition to occur and that different levels of net input power are required to achieve such negative E_r or ExB flow at different values of the individual parameters.

We note that recent results from ASDEX Upgrade indicate that the well of the edge E_r is driven by the contribution of the main ion diamagnetic term and that in order for the L-H transition to occur a critical value of the E_r well must be reached [37]. Before this can be tested on JET the uncertainty in the total edge E_r profiles needs to be reduced, in particular the contribution of the $v_{pol}\, B_{tor}$ term to the total field.

SUMMARY AND CONCLUSIONS

The exchange of plasma facing components in JET, from full C to all metal wall using the Be/W combination planned for ITER, has influenced several aspects of JET's operation, including H-mode confinement and access. The effects of the wall changes on the H-mode threshold have been studied by repeating L-H experiments previously run in JET-C. Experiments in JET-ILW show that P_{thr} is significantly influenced by variations both in plasma shaping and divertor configuration (strike point position). Therefore, to evaluate changes in P_{thr} due to wall composition, discharges with matched divertor geometry and plasma shaping, as well as same I_P/B_T, were used for the comparisons.

In JET-C with the currently installed MkII-HD divertor, P_{thr} varied monotonically with plasma density, in agreement with the ITPA scaling law. Following the installation of the ILW, a local minimum is observed in P_{thr} vs $\langle n_e \rangle$, with a low-density branch at increased power threshold and a high-density branch at reduced power threshold compared to the JET-C counterpart. At plasma densities above $n_{e,min}$ the H-mode power threshold is reduced by ~ 30%, and by ~ 40% when the bulk radiation is subtracted, in JET-ILW compared to JET-C, thus projecting favourably to ITER at face value. Interestingly, the L-H transition also occurs at lower edge electron temperature in JET-ILW, at a given edge density. A minimum in P_{thr} had already been observed in JET-C, but with closed divertor geometry, with septum in the private flux region (the MkII-GB divertor). These findings show that the occurrence of a minimum in P_{thr} is not a universal feature in JET, but is sensitive to both divertor geometry and divertor/wall material composition, pointing to a strong role played by SOL and divertor physics in the L-H transition. Therefore, extrapolation of results from present day tokamaks to ITER should be taken with care. The minimum density is found to increase roughly linearly with magnetic field in JET-ILW, $n_{e,min} \sim B_T^{4/5}$, and the power threshold at the minimum density to scale as $P_{sep,min} \sim B_T^{5/2}$.

Depending on the chosen divertor configuration, P_{thr} is observed to be up to a factor of two lower than the ITPA scaling law for densities above $n_{e,min}$. When the L-H data for different divertor configurations and plasma shapes are recast in terms of P_{sep} and Z_{eff} or subdivertor pressure (at constant edge density), a linear correlation is found, pointing to a possible role of these parameters in the L-H transition physics.

In JET-ILW, more input power is required than in JET-C to access the H-mode in low density ICRH heated plasmas, due to increased core radiation (W and Ni) at very low densities. On the other hand, after subtraction of the core radiation, similar values of P_{sep} are found at a given density

in NBI and ICRF heated plasmas at the L-H transition. Therefore, the net L-H power threshold is insensitive to the heating method (or weakly sensitive to variations of momentum input, as in the case of the JET-C results). In NBI-only discharges, L-mode core radiated power fractions are similar in JET-C and JET-ILW campaigns. Radiated power fractions in the divertor + X-point region are slightly reduced, both in NBI and ICRH plasmas, in JET-ILW relative to JET-C, in the L-mode phase up to the L-H transition.

However, in JET-ILW weaker edge transport barriers are formed after the L-H transition, in particular in the temperature profile, leading to H-modes with poorer confinement factors than in JET-C. The physics mechanisms underlying these changes are still under investigation.

Refurbishment of the JET edge CXRS diagnostic has resulted in higher quality impurity density profiles than previously, allowing analysis of the local impurity ion profiles across the L-H transition. Also in JET-ILW a shallow edge radial electric field well is observed at the L-H transition. Consistent with previous poloidal velocity measurements in JET, but in contrast with results from other tokamaks, the edge impurity ion poloidal velocity remains low, close to its L-mode values (0-5 km/s ±2-3 km/s), through the L-H transition and into the ELMy H-mode phase, with no measureable increase within the experimental uncertainties. The large error bars in v_{pol}, coupled to its low values, prevent the evaluation of the depth of the total E_r well and of the relative strength of diamagnetic vs poloidal velocity terms in the radial force balance of impurity ions. The diamagnetic term of the negative E_r well increases in magnitude across the L-H transition and into the H-mode phase in the radial region where the edge density and temperature transport barriers have formed and thus is likely to be correlated with the formation of the H-mode pedestal at the L-H transition. The edge toroidal rotation profile does not contribute to the depth of the negative E_r well and thus may not be correlated with the formation of the edge transport barrier in JET. The ion impurity diamagnetic term contribution to E_r at the L-H transition exhibits a minimum of order 1-3 kV/m, which, when recast in terms of the ExB flow, leads to a fairly constant value of ~ 0.5-1 km/s despite variations in edge density, toroidal magnetic field, divertor configuration or wall composition. On the other hand, the global analysis presented in this work shows significant variations in P_{thr} as a function of all these parameters. The 'local' and the 'global' observations could be linked under the assumption that a critical negative E_r value or EXB flow must be achieved for the L-H transition to occur and that different levels of net input power are required to achieve such critical E_r or ExB flow at different values of the individual parameters. However, increased accuracy needs to be achieved in the JET poloidal impurity ion flow measurements for a detailed evaluation of the depth of the edge E_r well and thus to test this assumption on JET.

ACKNOWLEDGMENTS

This work was supported by EURATOM and carried out within the framework of the European Fusion Development Agreement. The views and opinions expressed herein do not necessarily reflect those of the European Commission.

REFERENCES

[1]. G.F. Matthews *et al*., Physica Scripta **T145** 014001 (2011).

[2]. F. Romanelli and JET EFDA Contributors, Nuclear Fusion **53** (2013) 104002.

[3]. R. Neu et al., Physics of Plasmas **20** (2013) 056111.

[4]. C.F. Maggi et al., "The H-mode threshold in JET with the ITER-like wall", 39th EPS Conf. on Plasma Physics, Stockholm, 2012, O3-108, http://ocs.ciemat.es/epsicpp2012pap/pdf/O3.108.pdf

[5]. Y. Martin et al., JPCS **123** (2008) 012033.

[6]. S.J. Fielding et al., Plasma Physics and Controlled Fusion **38** (1996) 1091.

[7]. S.J. Fielding et al., Plasma Physics and Controlled Fusion **40** (1998) 731.

[8]. A. Hubbard et al., Plasma Physics and Controlled Fusion **40** (1998) 689.

[9]. Y. Ma et al., Nuclear Fusion **52** (2012) 023010.

[10]. T.N. Carlstrom and R.J. Groebner Physics of Plasmas **3** (1996) 1867.

[11]. L.D. Horton et al., "Dependence of the H-mode threshold on the JET divertor geometry", 26th EPS Conf. on Controlled Fusion and Plasma Physics (Maastricht) 1999.

[12]. Y. Andrew et al., Plasma Physics and Controlled Fusion, **48** (2006) 479.

[13]. F. Ryter et al., Nuclear Fusion **49** (2009) 062003.

[14]. F. Ryter et al., Nuclear Fusion **53** (2013) 113003.

[15]. A. Boboc et al., Review of Scientific Instruments **81** (2010) 10D538.

[16]. C.F. Maggi et al., "L-H threshold at low density and low momentum input in the JET tokamak", 38th EPS Conf. on Plasma Physics (Strasbourg) 2011, P4-061, http://ocs.ciemat.es/EPS2011PAP/pdf/P4.061.pdf

[17]. E. de la Luna et al., Review of Scientific Instruments **75** (2004) 3831.

[18]. R. Pasqualotto et al., Review of Scientific Instruments **75** (2004) 3891.

[19]. P. Gohil et al., Nuclear Fusion **50** (2010) 064011.

[20]. M. Mayoral et al., submitted to Nuclear Fusion.

[21]. T. Pütterich et al., Plasma Physics and Controlled Fusion **50** (2008) 085016.

[22]. S. Brezinsek et al., JNM **438** (2013) S303.

[23]. J. Wesson, 'Tokamaks', Clarendon Press, Oxford, 1997 (2nd Edition).

[24]. O Sauter et al., Physics of Plasmas **6** (1999) 2834 and O. Sauter et al., Physics of **9** (2002) 5140 (erratum).

[25]. C. Bourdelle et al, "L to H mode transition: on the role of Zeff", submitted to Nuclear Fusion Letter

[26]. U. Kreuzi et al., Review of Scientific Instruments **83** (2012) 10D728.

[27]. Y. Andrew et al., Plasma Physics and Controlled Fusion **46** (2004) A87.

[28]. A. Loarte et al., Physical Review Letters **83** (1999) 3657.

[29]. M Beurskens et al., "Global and pedestal confinement in JET with a metallic wall", accepted for publication in Nuclear Fusion.

[30]. C. Giroud et al., Nuclear Fusion **53** (2013) 113025.
[31]. Y. Andrew et al., Review of Scientific Instruments **77** (2006) 10E913.
[32]. T. M. Biewer et al., Review of Scientific Instruments **83** (2012) 10D505.
[33]. N.C. Hawkes et al., Plasma Physics and Controlled Fusion **38** (1996) 1261.
[34]. Y. Andrew et al., Europhysics Letters **83** (2008) 15003.
[35]. E. Viezzer et al., Nuclear Fusion **53** (2013) 053005.
[36]. R.J. Groebner and T.H. Osborne, Physics of Plasmas **5** (1998) 1800.
[37]. P. Sauter et al., Nuclear Fusion **52** (2012) 012001.
[38]. Y. Andrew et al., Plasma Physics and Controlled Fusion **50** (2008) 124053
[39]. M. Brix et al., Review of Scientific Instruments **81** (2010) 10D733

Configuration	**Plasma shape**	δ_U	δ_L
HT3L HT3R HT3	HIGH δ	~ 0.38	0.41 0.35 0.33
V5L V5	LOW δ	~ 0.19	0.40 0.33

Table 1: JET-ILW (MkII-HD) magnetic configurations explored in the L-H threshold experiments. The acronyms are as noted in the main text: three high δ shapes (HT3L, HT3R, HT3) have same upper triangularity $\delta_U \sim 0.38$ and decreasing lower triangularity δ_L as the outer strike point moves from left to right and the inner strike point moves down along the inner vertical plate; two low δ shapes (V5L, V5) have main plasma shape fixed at low upper triangularity $\delta_U \sim 0.19$ and δ_L varied to match the divertor configurations of HT3L and HT3R.

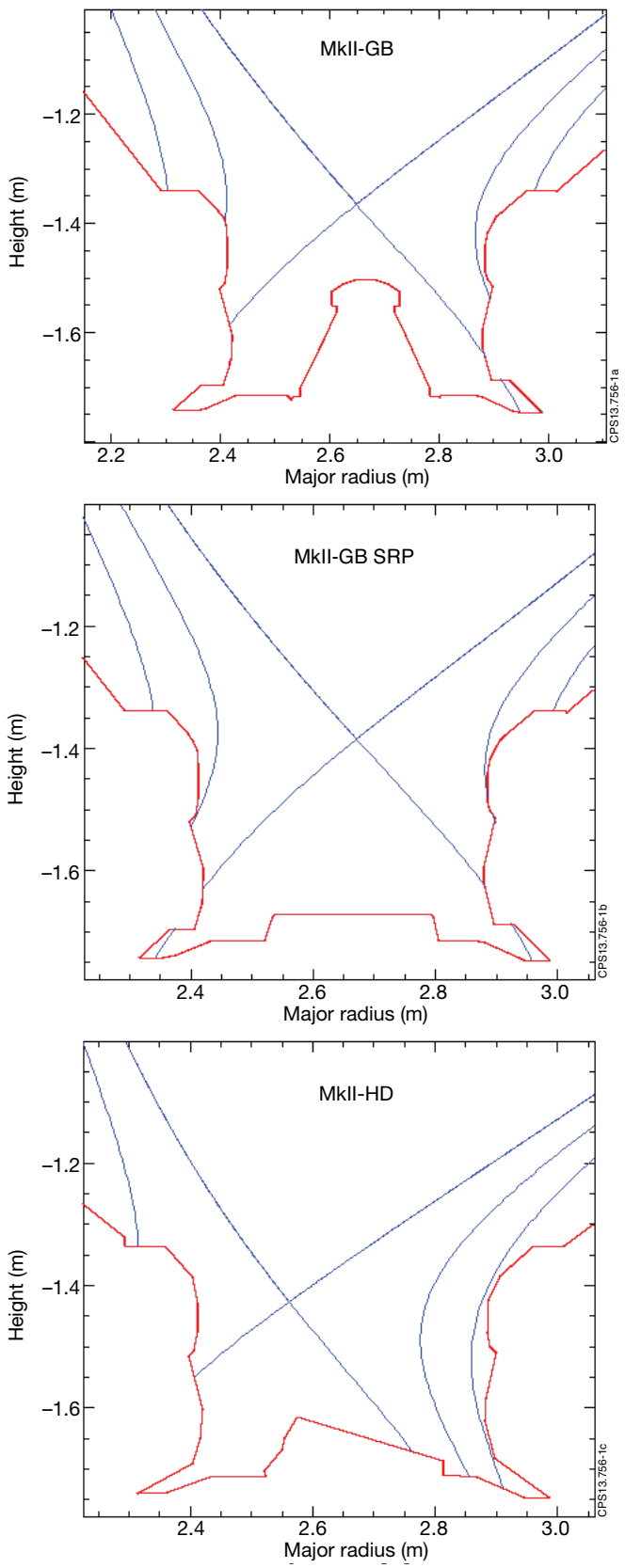

Figure 1. Poloidal cross sections of the JET-C divertor geometries discussed in this paper: (a) MkII-GB: minimum of P_{thr} vs density first observed; (b) MkII-GB SRP: minimum of P_{thr} vs density not observed; (c) MkII-HD: minimum of P_{thr} vs density not observed. This is also the divertor geometry currently installed in JET-ILW.

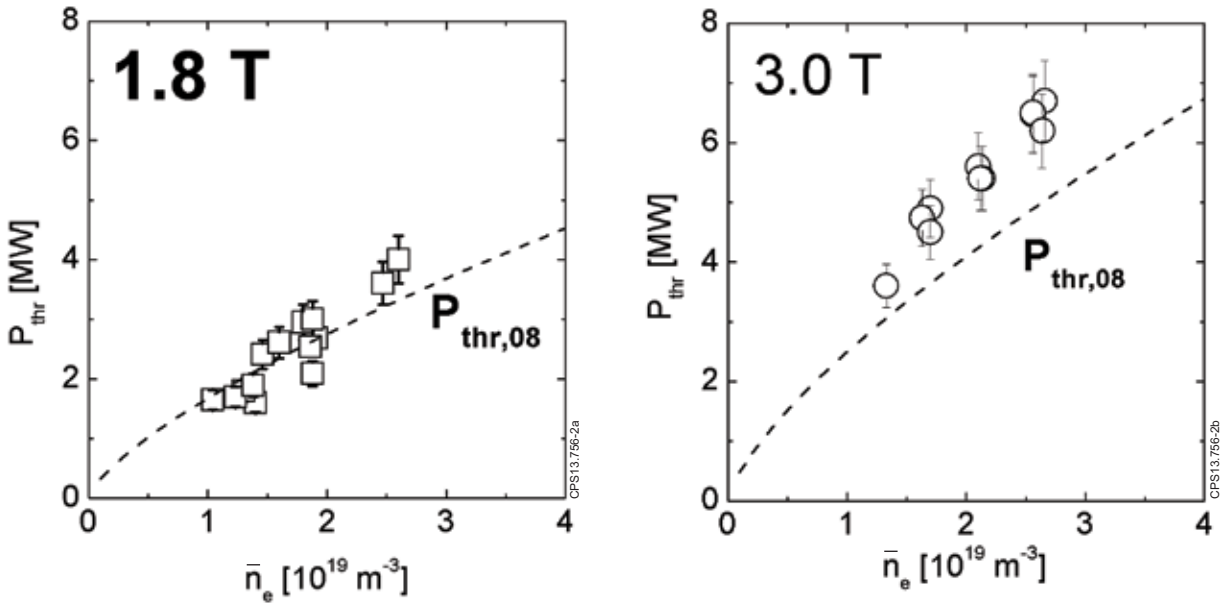

Figure 2. P_{thr} vs central line averaged density in JET-C with MkII-HD divertor geometry (a) at 1.8T/1.7MA, low and high triangularity (δ = 0.24 and 0.36) and (b) at 3.0T/2.75MA and high triangularity (δ = 0.36). The dashed curve denotes $P_{thr,08}$, the ITPA scaling law [5].

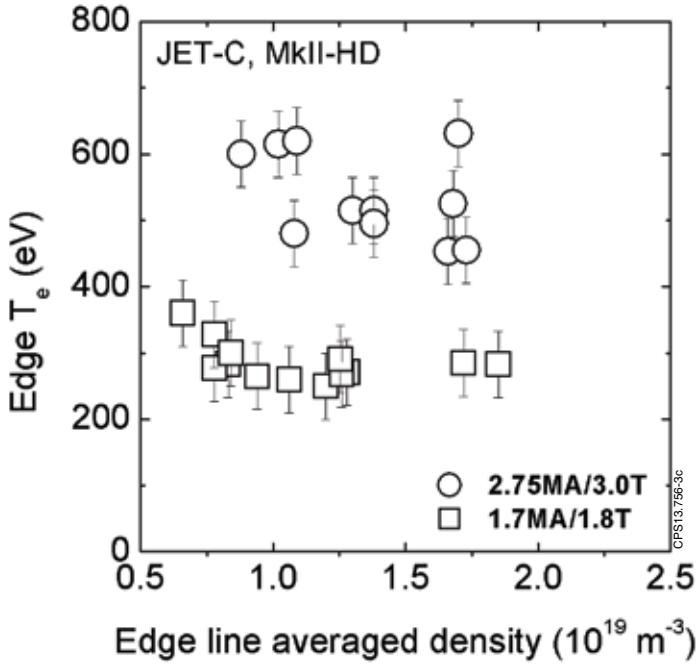

Figure 3. Edge T_e vs edge n_e at the L-H transition (in the radial location of the edge pedestal in the H-mode phase) during at 1.8T/1.7MA and 3.0T/2.75MA in JET-C and MkII-HD divertor geometry.

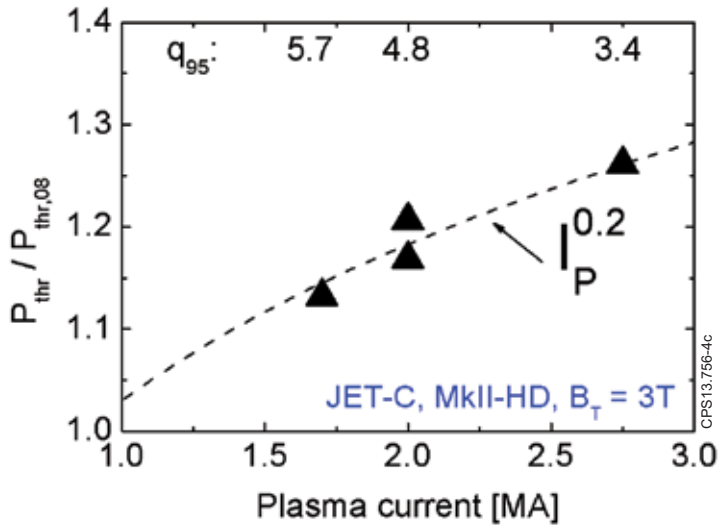

Figure 4. P_{thr} normalized to $P_{thr,08}$ vs I_P for the plasma current scan carried out in JET-C and MkII-HD divertor geometry at constant B_T = 3.0 T and $<n_e> \sim 2.0x10^{19}$ m^{-3}. The corresponding variation in q_{95} is also noted.

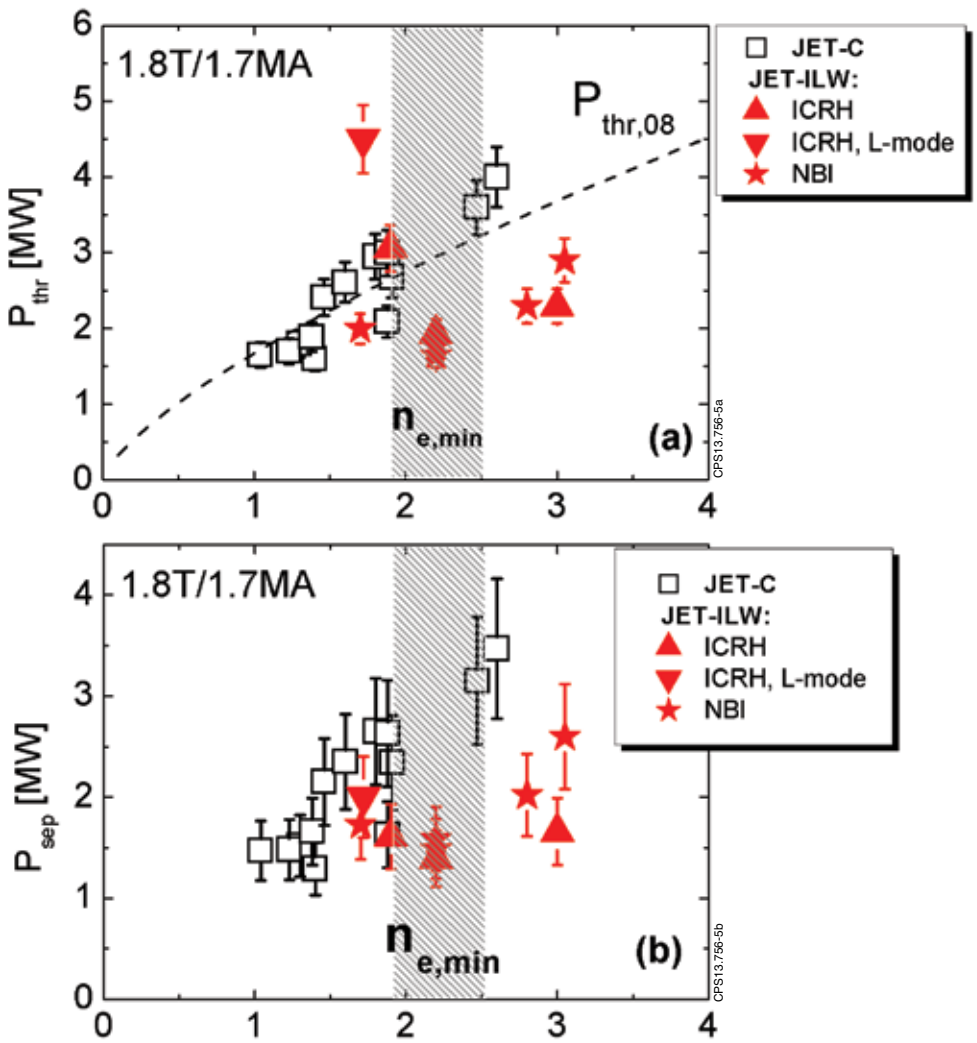

Figure 5. P_{thr} (a) and P_{sep} (b) vs central line averaged density at 1.8T/1.7MA for JET-C and JET-ILW datasets. The grey area marks the region of minimum n_e of P_{thr} and P_{sep}.

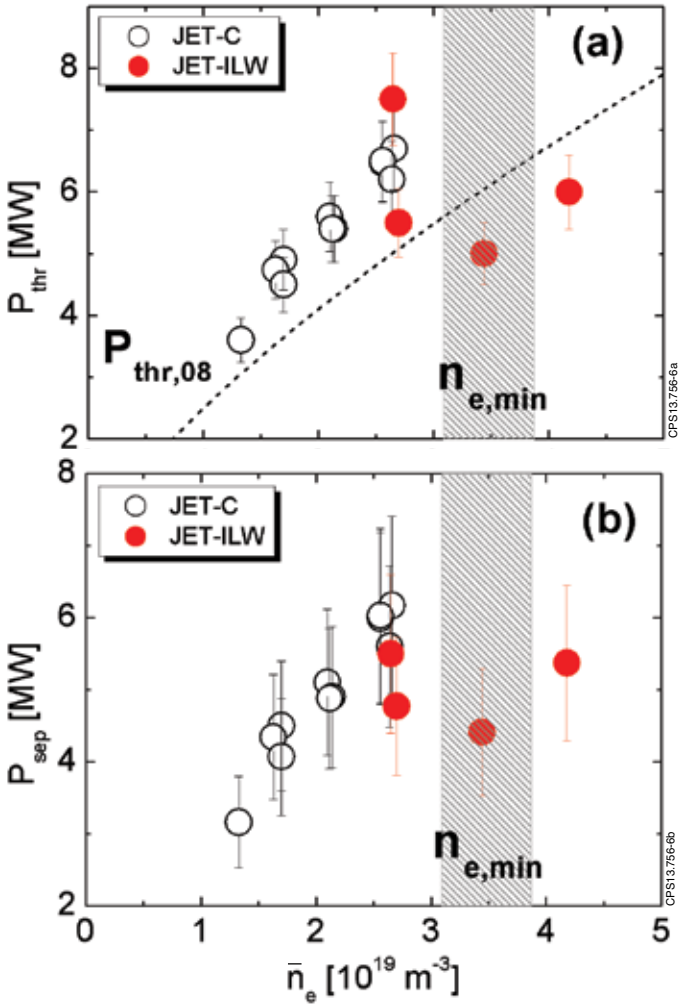

Figure 6. P_{thr} (a) and P_{sep} (b) vs central line averaged density at 3.0T/2.75MA and high δ for JET-C (NBI+ICRH) and JET-ILW (NBI only) datasets. The grey area marks the region of minimum n_e of P_{thr} and P_{sep}.

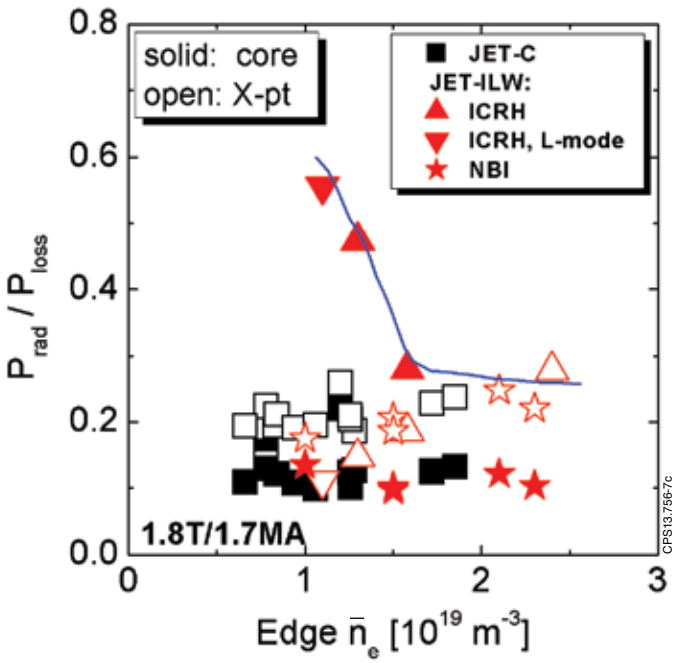

Figure 7. Radiated power (divertor + X-point: open symbols; core plasma: solid symbols) normalized to P_{loss} at the L-H transition for JET-C and JET-ILW at 1.8T/1.7 MA.

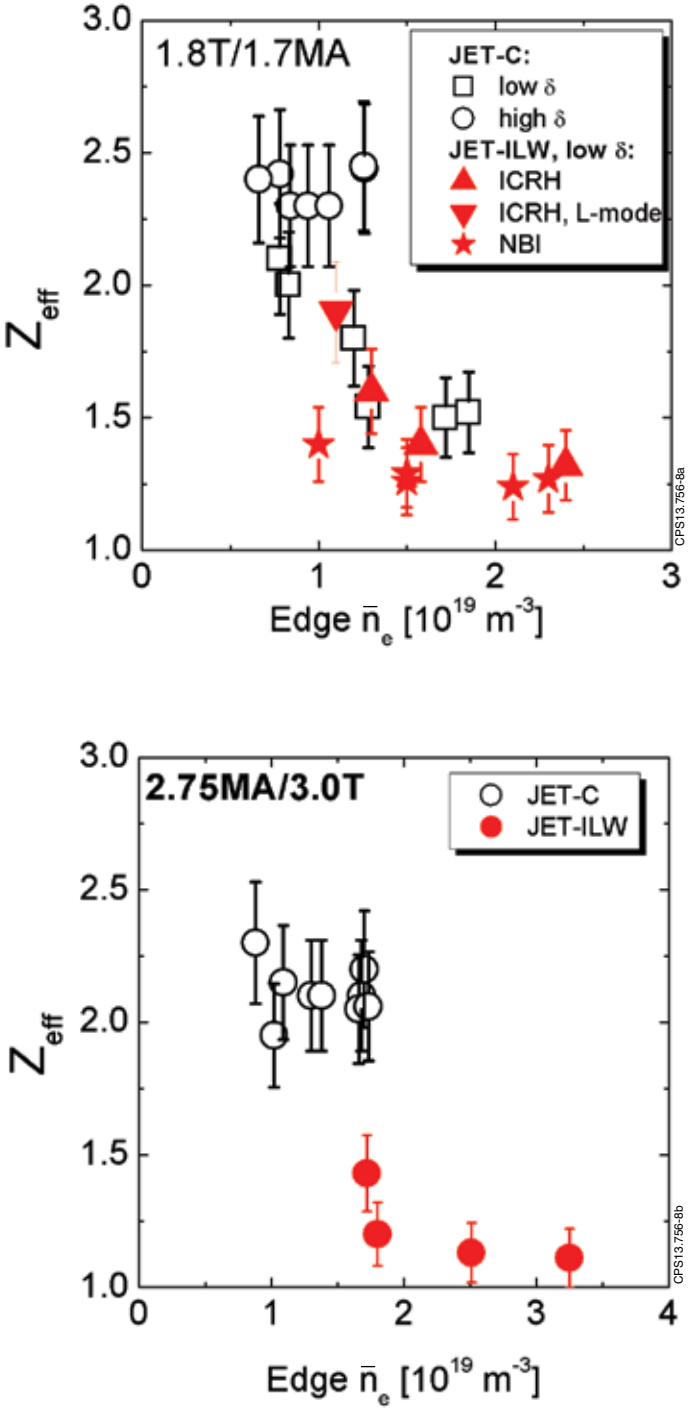

Figure 8. Z_{eff} vs edge line averaged density in JET-C and JET-ILW discharges at the time of the L-H transition for the datasets at (a) 1.8T and (b) 3.0T (high) of Figures 5 and 6. Statistical error bars are shown (10%), while a systematic error of 20% should be considered when comparing JET-C and JET-ILW datasets.

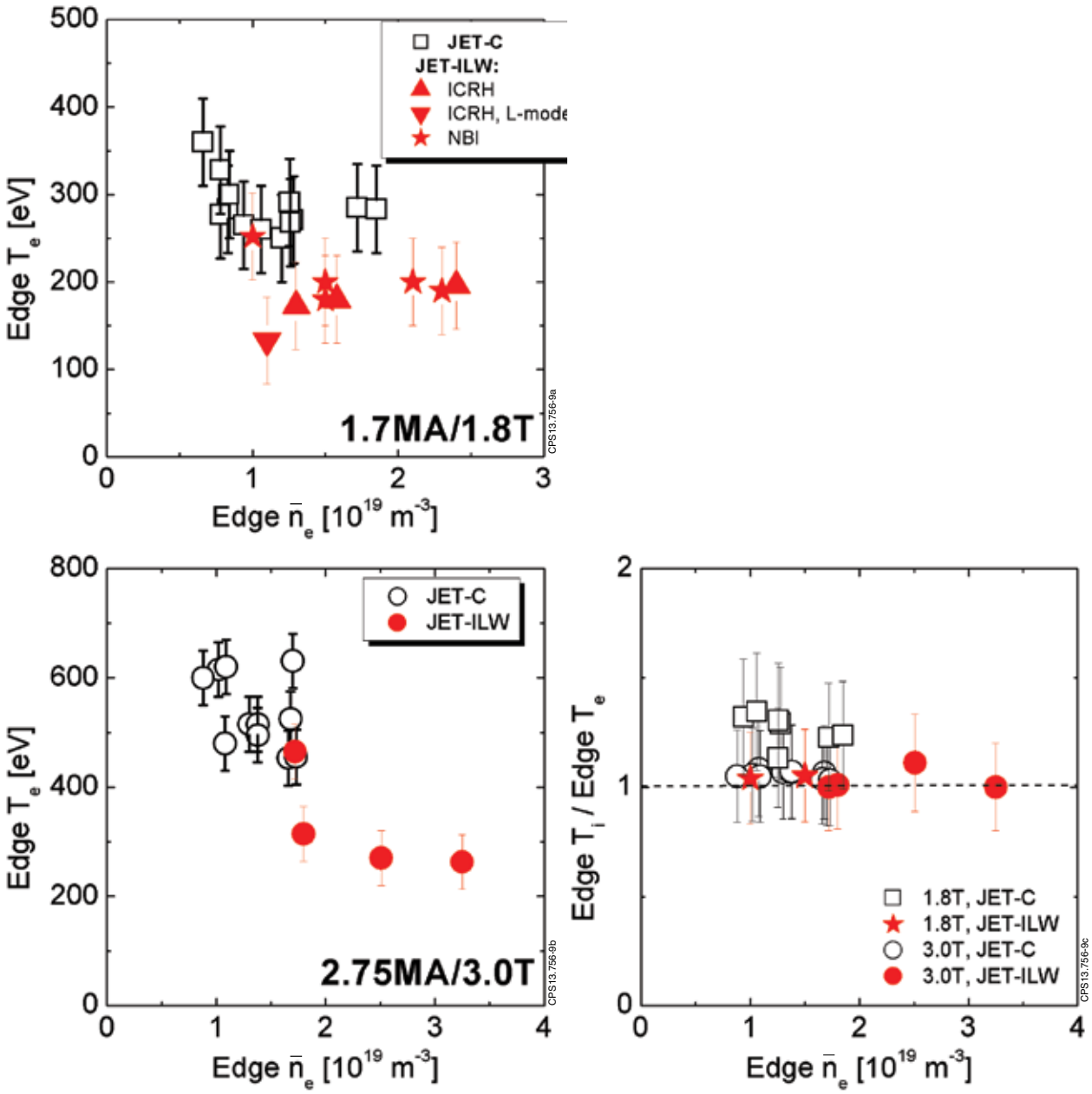

Figure 9. Edge T_e vs edge $<n_e>$ at the L-H transition for JET-C and JET-ILW: at 1.8T (a) and 3.0T (b); (c): ratio of edge T_i and edge T_e vs edge $<n_e>$ for the NBI heated discharges of the datasets of Figures (a) and (b) for which edge CXRS data are available.

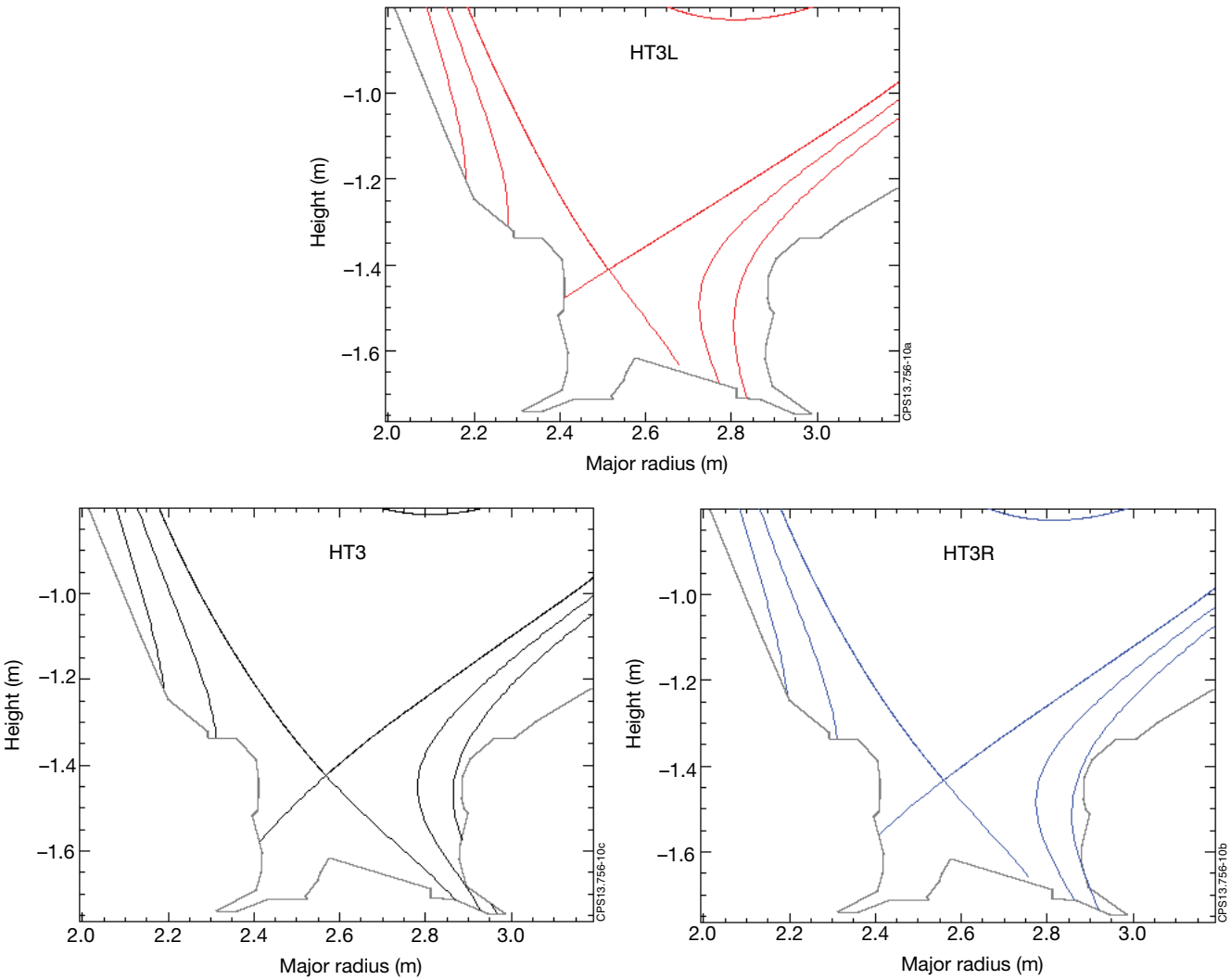

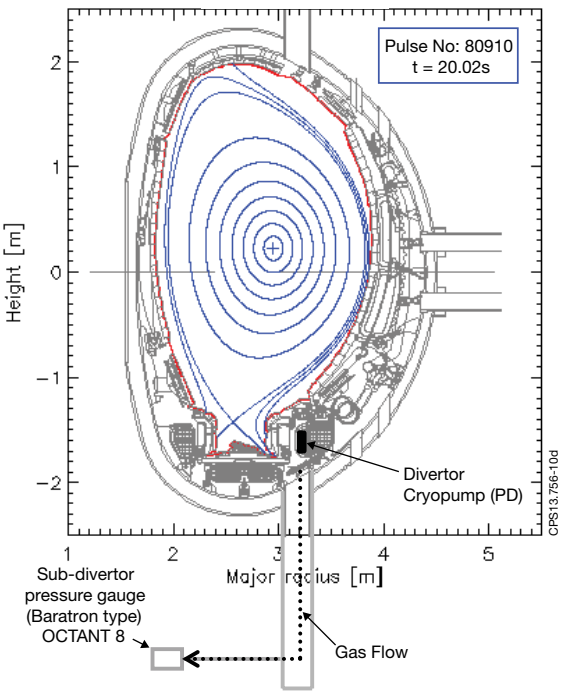

Figure 10. Divertor configurations of the 3 high triangularity plasma shapes explored in the L-H transition experiments with JET-ILW and MkII-HD geometry, as listed in Table 1. HT3L, HT3R, HT3: same $\delta_U \sim 0.38$ and decreasing δ_L as outer strike point moves from left to right of divertor floor and inner strike point moves downwards along the vertical target. Bottom right: geometrical location of the sub-divertor pressure gauge (baratron type) and of the divertor cryopump in JET.

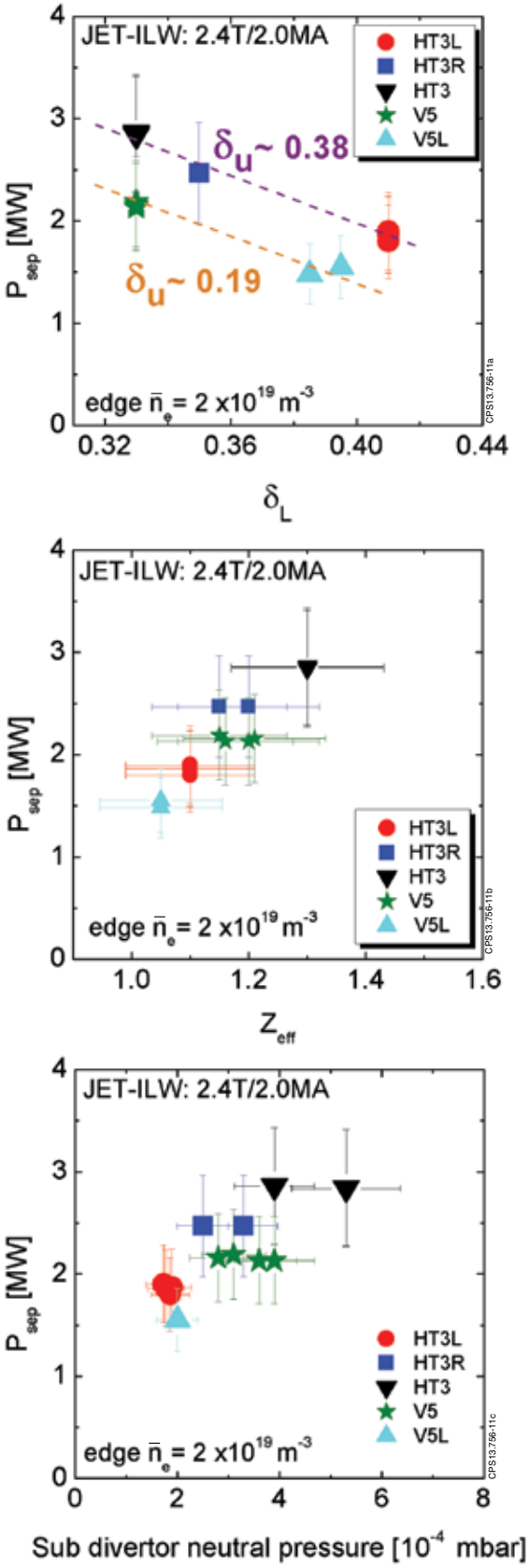

Figure 11. (a): Variation of P_{sep} with lower triangularity (δ_L) and upper triangularity (δ_U) in JET-ILW at 2.4T/2.0MA (ICRH heating only) and constant edge plasma density $<n_e> \sim 2 \times 10^{19}$ m^{-3}, which corresponds to $n_{e,min}$ at this B_T/I_P. The acronyms in the legend denote the five magnetic configurations of Table 1. (b): Variation of P_{sep} with Z_{eff} and (c) variation of P_{sep} with subdivertor neutral pressure at the L-H transition for the same set of discharges.

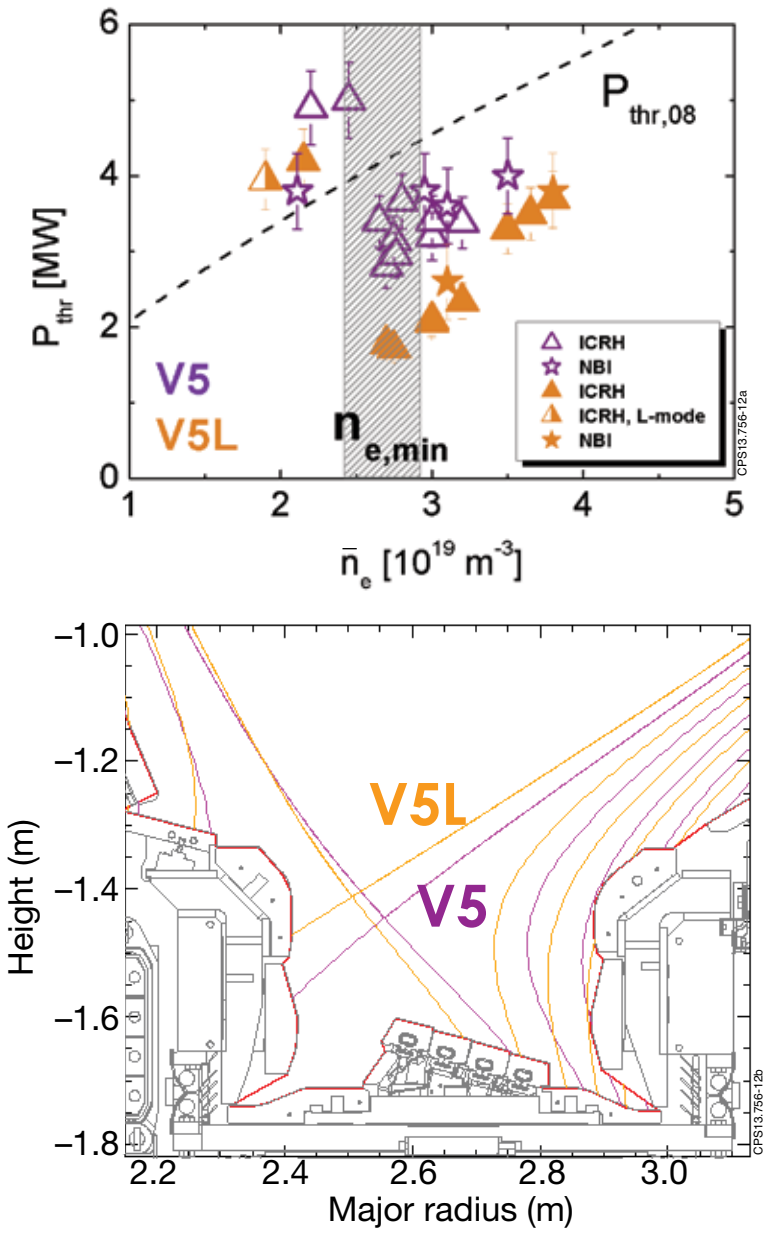

Figure 12. (a) Variation of P_{thr} with $<n_e>$ in JET-ILW (2.4T/2.0MA) at low δ shape ($\delta_U \sim 0.19$) for the two divertor configurations V5 and V5L (see Table 1) with different strike point positions, as shown in (b).

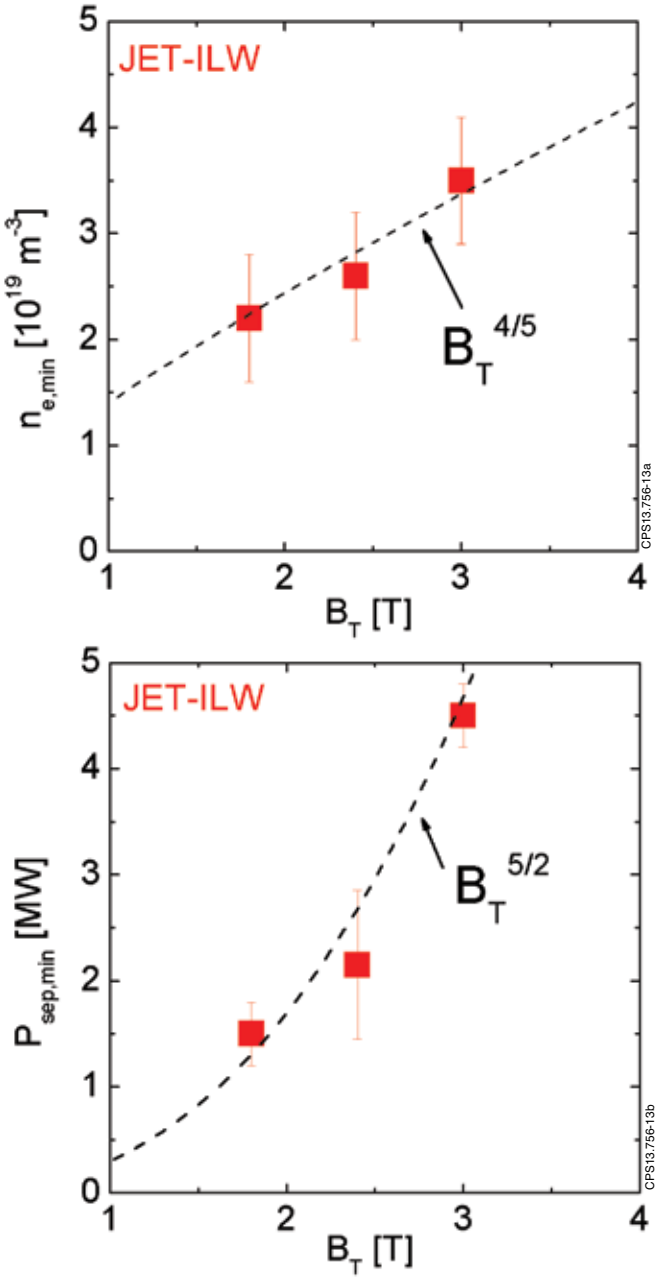

Figure 13. Increase of (a) $n_{e,min}$ and (b) $P_{sep,min}$ with magnetic field B_T in JET-ILW. The larger error bar in $P_{sep,min}$ at 2.4 T in Figure (b) reflects the measured variation in $P_{sep,min}$ when the divertor configuration is varied from V5 to V5L (see Figure 12) at this value of B_T.

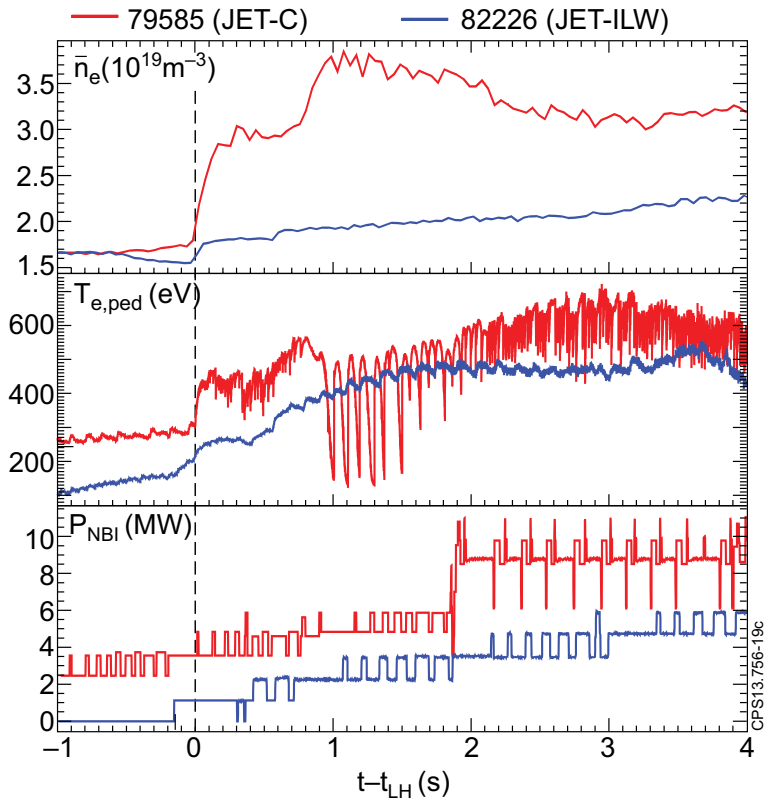

Figure 14. Time evolution across the L-H transition of two JET discharges at similar density (high density branch): JET-C (red) and JET-ILW (blue). From top to bottom panels: edge line averaged density; pedestal top temperature from ECE (with cut-off in the data for the JET-C wall shot between 0.9 and 2s) and auxiliary heating from NBI.

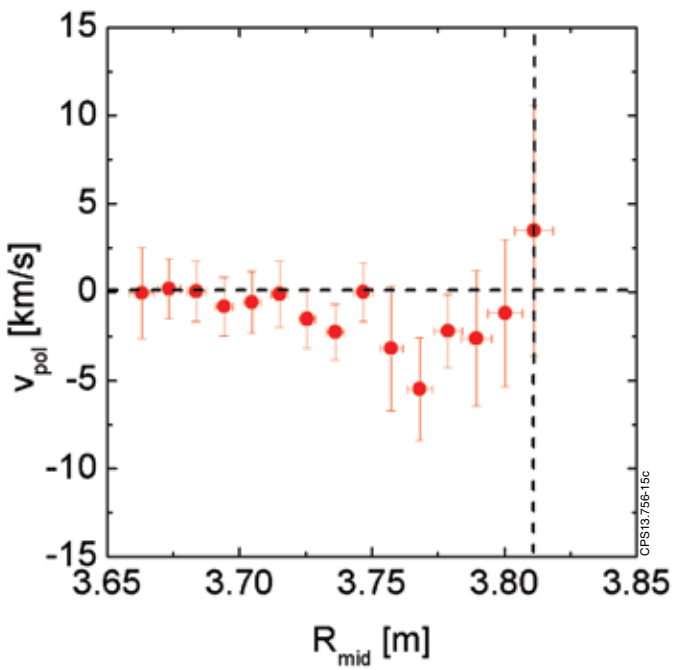

Figure 15. Edge poloidal velocity profile from C^{+6} CXRS, obtained by time averaging of the CX spectra over a 100 ms steady L-mode phase prior to the L-H transition (JET Pulse #83160). The sign convention is such that positive poloidal rotation is 'up', giving an outward vxB and a negative contribution to E_r. The poloidal rotation remains low also during the H-mode phase (see main text). The vertical dashed line marks the EFIT separatrix position, R_{mid} is the major radius at the magnetic axis.

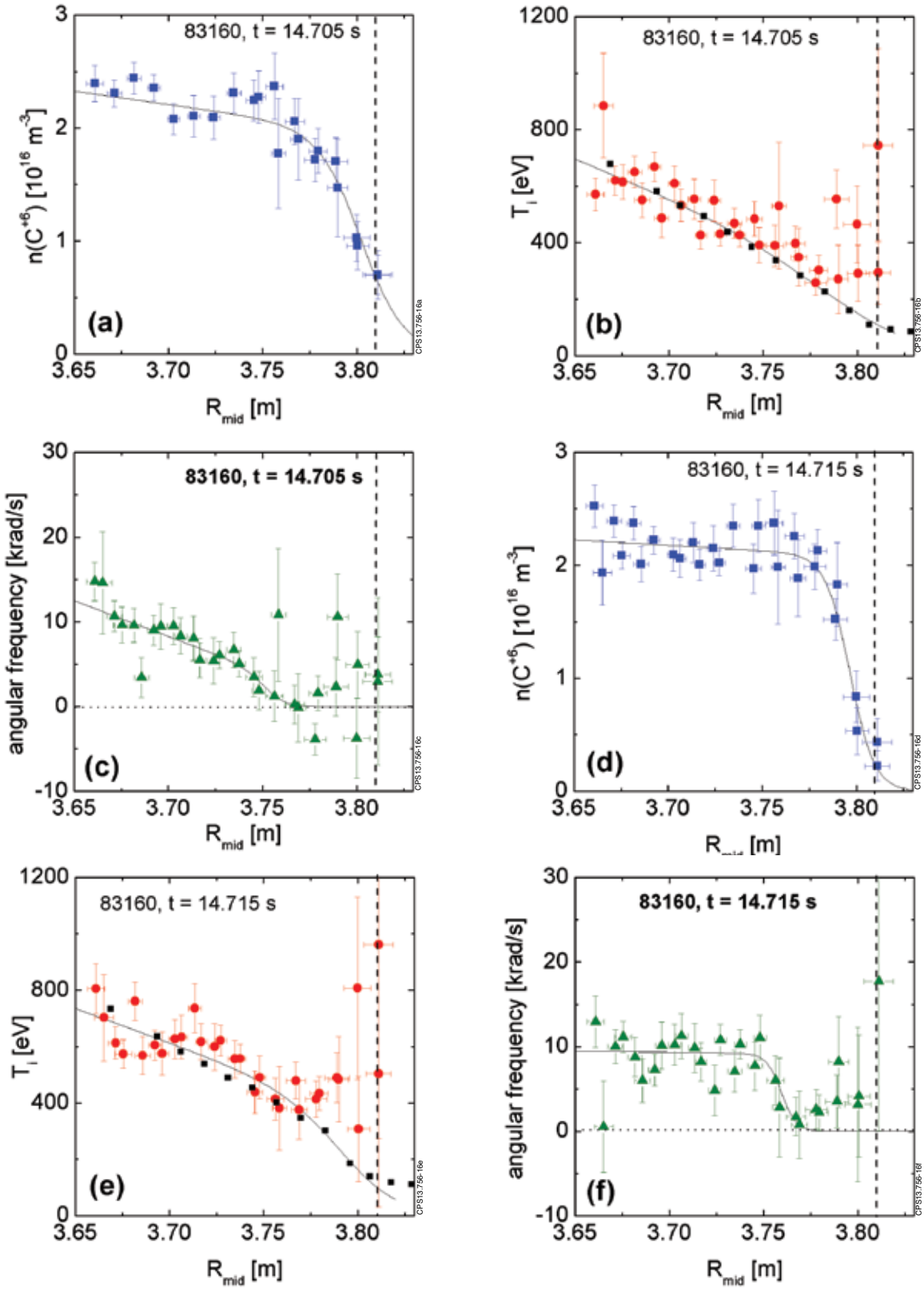

Figure 16. Profiles of (a) C^{+6} ion density, (b) temperature and (c) toroidal angular frequency (clockwise in a toroidal coordinate system, but here taken as positive according to the JET sign convention) at the L-H transition for JET pulse #83160 (JET-ILW, 3.0 T/2.75 MA, from the dataset of Figure 6), while panels (d), (e) and (f) show the evolution of the same profiles 10 ms after the L-H transition. Also plotted in panels (b) and (e) are the T_e profiles from ECE (black symbols). The solid lines are mtanh fits to the experimental data, the vertical dashed line marks the EFIT separatrix position, R_{mid} is the major radius at the magnetic axis.

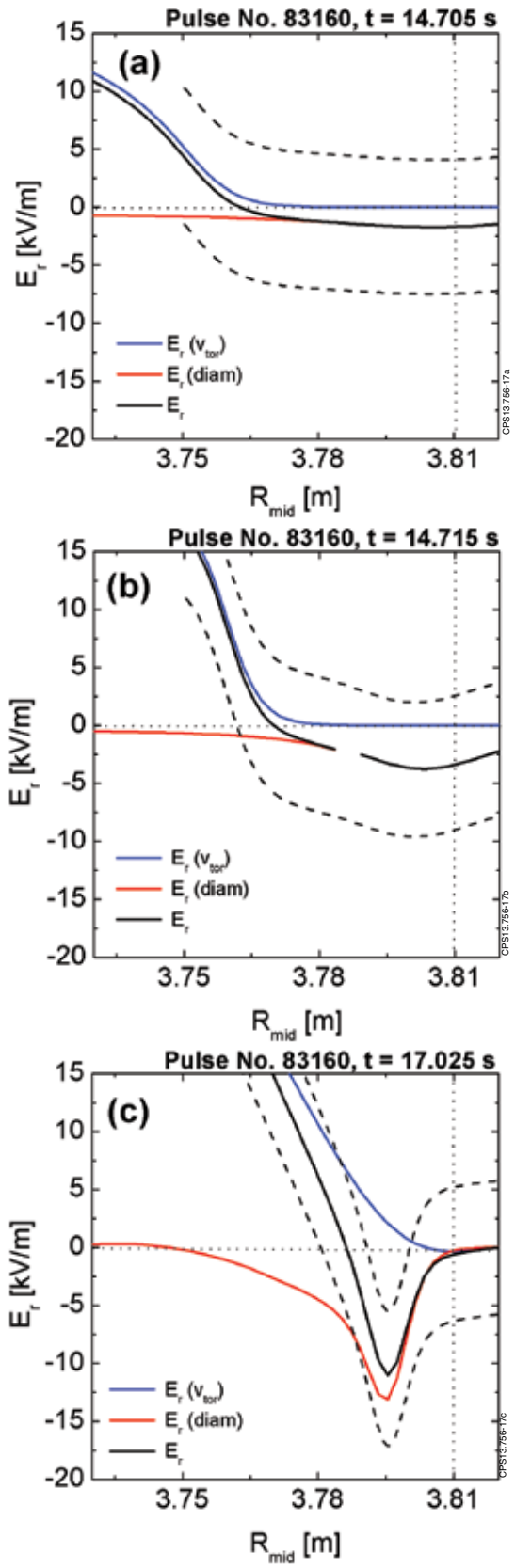

Figure 17. Edge E_r derived from the profiles of Figure 16, and assuming $v_{pol} = 0 \pm 2.5$ km/s (see text). Solid black line: E_r ($v_{pol} = 0$); dashed black lines: upper and lower bounds of E_r derived from the uncertainty in the v_{pol} measurement; solid red line: diamagnetic term; solid blue line: v_{tor} x B_{pol} term. (a) E_r at the L-H transition; (b) E_r 10 ms after the L-H transition and (c) E_r during the ELMy H-mode phase of the discharge. The vertical dashed lines mark the EFIT separatrix position, R_{mid} is the major radius at the magnetic axis.

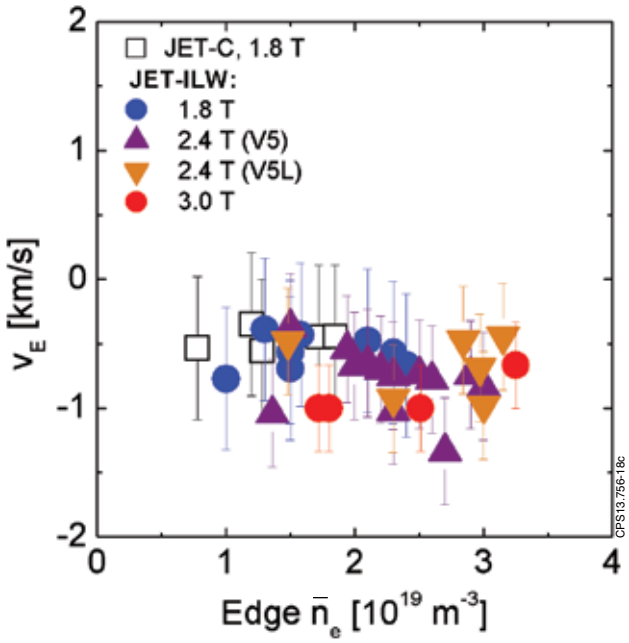

Figure 18. ExB flow v_E = (min $E_{r,dia}$)/B vs edge density for different values of B_T, wall composition and divertor strike point positions.